CBGL: Fast Monte Carlo Passive Global Localisation of 2D LIDAR Sensor

Alexandros Filotheou

***Abstract*— Given a LIDAR sensor's 2D measurement, at its core, CBGL disperses pose hypotheses within the map and ranks them ascendingly according to the value of the Cumulative Absolute Error per Ray (CAER) metric. The latter's inputs comprise the input measurement and the map-scan captured from each hypothesis. This produces a ɾ(ank)-field which may be used to estimate the pose of the sensor (a) quickly due to the metric's low computational complexity, and (b) accurately due to (i) proportionality between the pose estimate error and the value of the metric for pose estimates in a neighbourhood of the sensor's pose, and (ii) lack of disproportionality outside of that neighbourhood. The source code is available for download.**

***Index Terms*— global localisation, 2D LIDAR, monte carlo, scan–to–map-scan matching**

I. Introduction

This paper addresses the problem of Passive Global Localisation of a 2D LIDAR sensor, i.e. the estimation of its location and orientation within a given map, under complete locational and orientational uncertainty, without prescribing motion commands (to the mobile robot that the sensor is assumed mounted to) for further knowledge acquisition. The problem is formalised in Problem P:

Problem P. Let the unknown pose of an immobile 2D range sensor whose angular range is λ be $\boldsymbol{p}(\boldsymbol{l},\theta)$, $\boldsymbol{l} = (x, y)$, with respect to the reference frame of map $\boldsymbol{M}$. Let the range sensor measure range scan $\mathcal{S}_R$. The objective is the estimation of $\boldsymbol{p}$ given $\boldsymbol{M}$, λ, and $\mathcal{S}_R$.

The rest of the paper is structured as follows: Section II provides necessary definitions and the notation employed. Section III gives a brief review of the literature of solutions to problem P, and the relation of the proposed method to them. The latter's methodology is presented in section IV, its evaluation in section V, and its limitations in section VI. Section VII concludes this study.

II. Definitions and Notation

Let $\mathcal{A} = \{\alpha_i : \alpha_i \in \mathbb{R}\}$, $i \in \mathtt{I} = \langle 0, 1, \ldots, n-1\rangle$, denote a set of n elements, $\langle\cdot\rangle$ denote an ordered set, $\mathcal{A}_\uparrow$ the set $\mathcal{A}$ ordered in ascending order, the bracket notation $\mathcal{A}[\mathtt{I}] = \mathcal{A}$ denote indexing, and notation $\mathcal{A}_{k:l}$, $0 \leq k \leq l$, denote limited indexing: $\mathcal{A}_{k:l} = \{\mathcal{A}[k], \mathcal{A}[k+1], \ldots, \mathcal{A}[l]\}$.

Definition I. *Range scan captured from a 2D LIDAR sensor.*—A conventional 2D LIDAR sensor provides a finite number of ranges, i.e. distances to objects within its range, on a horizontal cross-section of its environment, at regular angular and temporal intervals, over a defined angular range [1]. A range scan $\mathcal{S}$, consisting of N_s rays over an angular range λ, is an ordered map $\mathcal{S} : \Theta \to \mathbb{R}_{\geq 0}$, $\Theta = \{\theta_n \in [-\frac{\lambda}{2}, +\frac{\lambda}{2}) : \theta_n = -\frac{\lambda}{2} + \lambda\frac{n}{N_s}, n = 0, 1, \ldots, N_s - 1\}$. Angles θ_n are expressed relative to the sensor's heading, in the sensor's frame of reference.

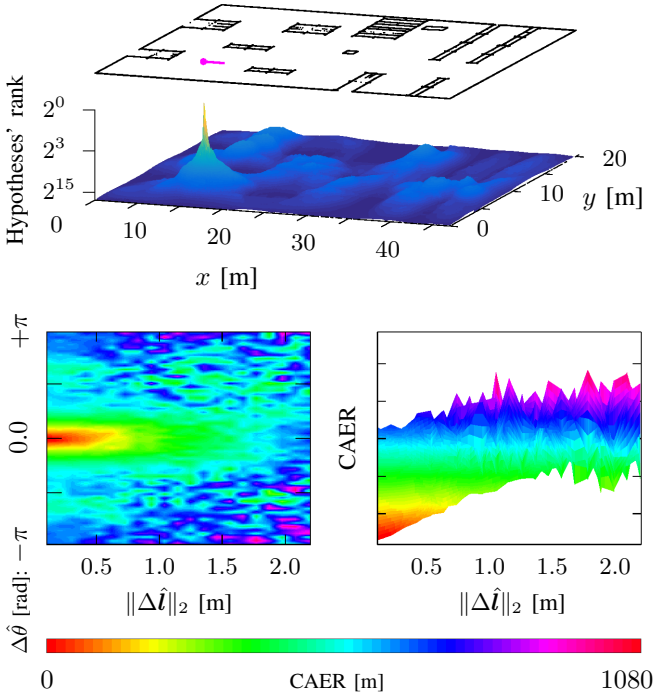

Fig. 1: Top: a map of an environment, the pose of a panoramic 2D LIDAR sensor (magenta), and the corresponding CAER rank field below them. Bottom: distribution of CAER values by location $\Delta\hat{\boldsymbol{l}}$ and orientation error $\Delta\hat{\theta}$ of all sensor pose hypotheses corresponding to the rank field above, for estimate position errors up to 2.0 m. In this example 10^6 hypotheses are dispersed randomly in the free space of a map with area 735 m^2, for 100 independent trials; CBGL's maximum location error and maximum execution time are, respectively, 0.062 m and 8.8 sec

Definition II. *Map-scan.*—A map-scan is a virtual scan that encapsulates the same pieces of information as a scan derived from a physical sensor. Only their underlying operating principle is different due to the fact the map-scan refers to distances to the boundaries of a point-set, referred to as the map, rather than within a real environment. A map-scan $\mathcal{S}_V^{\boldsymbol{M}}(\hat{\boldsymbol{p}})$ is derived by means of locating intersections of rays emanating from the estimate of the sensor's pose estimate $\hat{\boldsymbol{p}}$ and the boundaries of the map $\boldsymbol{M}$.

Definition III. *CAER as metric.*—Let $\mathcal{S}_p$ and $\mathcal{S}_q$ be two range scans, equal in angular range λ and size N_s. The value of the Cumulative Absolute Error per Ray (CAER) metric

$\psi \in \mathbb{R}_{\geq 0}$ between $\mathcal{S}_p$ and $\mathcal{S}_q$ is given by

$$\psi(\mathcal{S}_p, \mathcal{S}_q) \triangleq \sum_{n=0}^{N_s-1} \Big| \mathcal{S}_p[n] - \mathcal{S}_q[n] \Big| \tag{1}$$

Definition IV. *CAER as field.*—A ψ-field on map $\boldsymbol{M}$ $f_{\psi}^{\boldsymbol{M}} : \mathbb{R}^2 \times [-\pi, +\pi) \rightarrow \mathbb{R}_{\geq 0}$ is a mappping of 3D pose configurations $\hat{\boldsymbol{p}}(\hat{x}, \hat{y}, \hat{\theta})$ to CAER values (def. III) such that if $\psi(\mathcal{S}_R, \mathcal{S}_V^{\boldsymbol{M}}(\hat{\boldsymbol{p}})) = c$ then $f_{\psi}^{\boldsymbol{M}}(\hat{\boldsymbol{p}}) = c$. In other words a CAER field is produced by computing the value of the CAER metric between a range scan $\mathcal{S}_R$ (def. I) and a map-scan $\mathcal{S}_V^{\boldsymbol{M}}(\hat{\boldsymbol{p}})$ captured from pose configuration $\hat{\boldsymbol{p}}$ within map $\boldsymbol{M}$ (def. II).

Definition V. *Rank field.*—Let $f_{\psi}^{\boldsymbol{M}}$ be a ψ-field on map $\boldsymbol{M}$ and $\mathcal{P} = \{\hat{\boldsymbol{p}}_i\}$, $i \in \mathtt{I} = \langle 0, 1, \ldots, |\mathcal{P}| - 1 \rangle$, be a set of 3D pose configurations within map $\boldsymbol{M}$, such that $f_{\psi}^{\boldsymbol{M}}(\mathcal{P}) = \Psi$. Let $\mathtt{I}^*$ be the set of indices such that $\Psi[\mathtt{I}^*] = \Psi_{\uparrow}$. A $\mathtt{r}$-field on map $\boldsymbol{M}$ $f_{\mathtt{r}}^{\boldsymbol{M}} : \mathbb{R}^2 \times [-\pi, +\pi) \rightarrow \mathbb{Z}_{\geq 0}$ is a mapping of 3D pose configurations $\mathcal{P}$ to non-negative integers such that if $f_{\psi}^{\boldsymbol{M}}(\mathcal{P}) = f_{\psi}^{\boldsymbol{M}}(\mathcal{P}[\mathtt{I}]) = \Psi$ then $f_{\mathtt{r}}^{\boldsymbol{M}}(\mathcal{P}[\mathtt{I}^*]) = \mathtt{I}$. In other words a rank field maps the elements of pose estimate set $\{\hat{\boldsymbol{p}}_i\}$ to the ranks $\mathtt{I}^*$ of their corresponding CAER values in hierarchy $\Psi_{\uparrow}$.

Definition VI. *Field densities*.—The locational and angular density, $d_{\boldsymbol{l}}$ and d_{α} respectively, of a ψ- or r-field express, correspondingly, the number of pose estimates per unit area of space and per angular cycle, where $d_{\boldsymbol{l}}, d_{\alpha} \in \mathbb{N}$.

Definition VII. *Admissibility of solution*.—A pose estimate $\hat{\boldsymbol{p}}(\hat{x}, \hat{y}, \hat{\theta}) \in \mathbb{R}^2 \times [-\pi, +\pi)$ may be deemed an admissible solution to Problem P iff $\|\boldsymbol{l} - \hat{\boldsymbol{l}}\|_2 \leq \delta_{\boldsymbol{l}}$ and $|\theta - \hat{\theta}| \leq \delta_{\theta}$ and $\|\boldsymbol{p} - \hat{\boldsymbol{p}}\|_2 \leq \delta$, where $\delta_{\boldsymbol{l}}, \delta_{\theta}, \delta \in \mathbb{R}_{>0}$: $\delta_{\boldsymbol{l}}^2 + \delta_{\theta}^2 = \delta^2$.

III. Related Work

The literature concerning the solution to the problem of global localisation with the use of a 2D LIDAR sensor is rich; a brief overview is given below.

In broad terms global localisation approaches may be divided into two categories: (a) approaches that operate in feature space, that is, methods that extract features from measurements and the map and then establishing correspondences between them, and (b) approaches that directly exploit only raw measurements. In the latter category a number of global localisation methods solve the problem in an iterative Bayesian Monte Carlo fashion, i.e. by dispersing hypotheses within the map and updating the belief of the robot's pose by incorporating new measurements as it moves until estimate convergence [2]–[6]. However, the requirement of motion (a) may give rise to safety concerns (the robot may not even be visible), and (b) increases estimation time. The Monte Carlo method proposed in this article operates directly in measurement space as well but, in contrast, it does not require motion or more than one measurement. As a result CBGL is a single-shot global localisation approach that is executable in less time compared to previous Monte Carlo approaches.

Research on the former category has been more extensive due to the richness, appropriateness, adaptability, and efficacy of methods originated in the computer vision field. Relevant methods mainly perform detection of key-points in a measurement, followed by the calculation of a distinctive signature, which is then matched to similarly- and pre-computed place-signatures [7]–[13]. In principle, however, unstructured environments cannot be relied upon for the existence of features, due to their complete absence or their sparse and fortuitous distribution (although Deep Neural Network approaches have demonstrated increased performance in place recognition with the use of 3D LIDARs [14]–[16]). Structured environments on the other hand manifest different features depending on the particularities of the environment. In any case, features may be present but not in a sufficiently undisturbed state due to sensor noise or map-to-environment mismatch.

The motivation of the proposed method originates from seeking to achieve a greater degree of universality, reliability, and portability across multiple and disparate environments, by not making a priori assumptions on environment structure, and by aiming to minimise requirements on resources (number and types of sensors; number of measurements; time). The proposed method is most akin to the two tested methods in [17]: all three are single-shot 2D LIDAR-based Monte Carlo approaches, but CBGL computes a measure of the alignment of (a) the measurement to (b) the virtual scan captured from each hypothesis *before* scan–to–map-scan matching a subset of the most-aligned poses to the measurement. As a consequence it is able to process more hypotheses in less time, resulting in (a) an improvement over the number of correctly estimated locations and, most starkly, (b) execution time, being able to compete against (traditionally faster) feature-based approaches.

A recent and comprehensive survey on global localisation may be found in [18].

IV. The CBGL method

A. Motivation

The proposed method's motivation lies in the simple but powerful fact that is, in general, exhibited through figure 1: Assume a pose estimate residing in a neighbourhood of a 2D LIDAR sensor's pose within a given map; then the value of the CAER metric between the scan measured by the sensor and the map-scan captured from the estimate within the map is simultaneously proportional to both the estimate's location error and orientation error. Formally the proposed method's foundations rest on Observation O:

Observation O. It may be observed that there are conditions such that Hypothesis H stands true.

Hypothesis H. There exists $\hat{\boldsymbol{p}} \in \mathbb{R}^2 \times [-\pi, +\pi)$ such that $\hat{\boldsymbol{p}} \in \mathcal{V} : \|\boldsymbol{p} - \hat{\boldsymbol{p}}\|_2 \leq \delta \leq \delta_0$ is an admissible pose estimate solution to Problem P (def. VII), where set $\mathcal{V}$ and δ_0 are defined by Conjecture C.

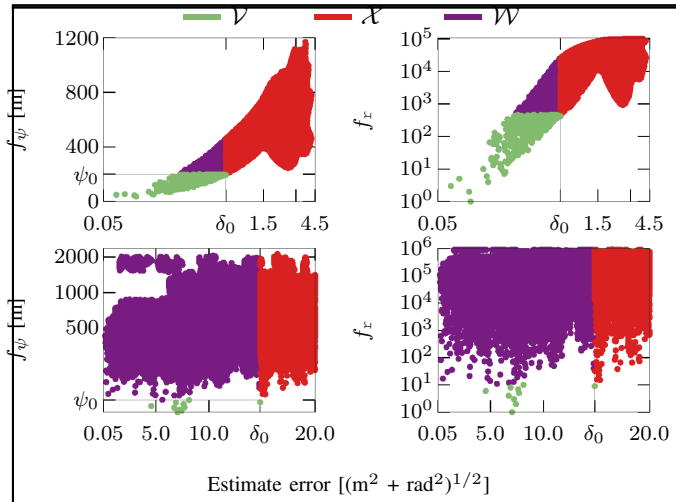

Fig. 2: The ψ-field (left) and $\mathtt{r}$-field (right) of a configuration where Observation O may (top) and may not (bottom) be made for $\delta \leq \delta_0$. Bottom: in contrast to the top row, set $\mathcal{V}$ is empty of admissible pose estimates for $\delta < 4.5$ $(\text{m}^2 + \text{rad}^2)^{1/2}$. The effect is produced in environment WILLOWGARAGE (pose $\boldsymbol{p}_i^G$; subsection V-B) due to (a) the repetition of the immediate environment of the sensor more than once in the given map, and (b) the non-panoramic angular range of the sensor

Conjecture C. Let the unknown pose of a 2D range sensor measuring range scan $\mathcal{S}_R$ (def. I) be $\boldsymbol{p}(x, y, \theta)$ with respect to the reference frame of map $\boldsymbol{M}$. Let $\mathcal{H}$ be a set of pose hypotheses within the free (i.e. traversable) space of $\boldsymbol{M}$: $\mathcal{H} = \{\hat{\boldsymbol{p}}_i(\hat{x}_i, \hat{y}_i, \hat{\theta}_i)\} \subseteq \mathtt{free}(\boldsymbol{M})$, $i \in \mathtt{I} = \langle 0, 1, \ldots, |\mathcal{H}| - 1\rangle$. Let $f_\psi^{\boldsymbol{M}}$ be the ψ-field on $\boldsymbol{M}$ (def. IV) such that $f_\psi^{\boldsymbol{M}}(\mathcal{H}) = \Psi$. Let the field's locational and orientational densities be $d_{\boldsymbol{l}}$ and d_α. Let $\hat{\boldsymbol{p}}_\omega \in \mathcal{H}$ and $\psi_0, \delta_0 \in \mathbb{R}_{>0}$ such that $f_\psi^{\boldsymbol{M}}(\hat{\boldsymbol{p}}_\omega) = \psi_0$ and $\|\boldsymbol{p} - \hat{\boldsymbol{p}}_j\|_2 \leq \delta_0$ for all $\hat{\boldsymbol{p}}_j \in \mathcal{H} : f_\psi^{\boldsymbol{M}}(\hat{\boldsymbol{p}}_j) \leq \psi_0$. Let now $\mathcal{V} = \{\hat{\boldsymbol{p}}_i \in \mathcal{H} : f_\psi^{\boldsymbol{M}}(\hat{\boldsymbol{p}}_i) \leq \psi_0, \|\boldsymbol{p} - \hat{\boldsymbol{p}}_i\|_2 \leq \delta_0\}$. Without loss of generality there exist $d_{\boldsymbol{l}}, d_\alpha$, and ψ_0, δ_0 such that for all $\hat{\boldsymbol{p}}_\mathcal{V} \in \mathcal{V}$:

$$f_\psi^{\boldsymbol{M}}(\hat{\boldsymbol{p}}_\mathcal{V}) < f_\psi^{\boldsymbol{M}}(\hat{\boldsymbol{p}}) \quad \Leftrightarrow \quad \|\boldsymbol{p} - \hat{\boldsymbol{p}}_\mathcal{V}\|_2 < \|\boldsymbol{p} - \hat{\boldsymbol{p}}\|_2$$

for any $\hat{\boldsymbol{p}} \in \mathcal{X} = \mathcal{H} \setminus \mathcal{V} : \|\boldsymbol{p} - \hat{\boldsymbol{p}}\|_2 > \delta_0$.

Remark I. The composition of $\mathcal{H} = \mathcal{V} \cup \mathcal{X} \cup \mathcal{W}$, where $\mathcal{W} = \hat{\boldsymbol{p}} \in \mathcal{H} \setminus \mathcal{V} : \|\boldsymbol{p} - \hat{\boldsymbol{p}}\|_2 \leq \delta_0$. With regard to the elements of set $\mathcal{W}$: if a global localisation system's output was pose $\hat{\boldsymbol{p}}_\mathcal{W} \in \mathcal{W}$ then, in the language of classification, $\hat{\boldsymbol{p}}_\mathcal{W}$ would constitute a false negative: it may be that $f_\psi^{\boldsymbol{M}}(\hat{\boldsymbol{p}}_\mathcal{W}) > f_\psi^{\boldsymbol{M}}(\hat{\boldsymbol{p}}_\mathcal{X})$ but with regard to the pose error: $\|\boldsymbol{p} - \hat{\boldsymbol{p}}_\mathcal{X}\|_2 \leq \delta_0$ and $\|\boldsymbol{p} - \hat{\boldsymbol{p}}_\mathcal{W}\|_2 \leq \delta_0$.

In simple terms Conjecture C states that, in general, given a dense enough set of pose hypotheses $\mathcal{H}$ over a map $\boldsymbol{M}$, it is possible to partition $\mathcal{H}$ into such (non-empty) sets $\mathcal{V}$, $\mathcal{X}$, and $\mathcal{W}$ that the error of pose estimates in set $\mathcal{V}$ and their corresponding CAER values are simultaneously lower than those of estimates in set $\mathcal{X}$. Hypothesis H restrictingly states that $\mathcal{V}$ is populated by a pose estimate whose error is such that it is deemed an admissible solution to Problem P. Figure 2 (top) shows an example configuration where Hypothesis H stands true for some $\delta \leq \delta_0 = 0.50$ $(\text{m}^2 + \text{rad}^2)^{1/2}$.

B. The CBGL System

In the same vein as Hypothesis H assume the $\mathtt{r}$-field $f_\mathtt{r}^{\boldsymbol{M}}(\mathcal{H})$ corresponding to the ψ-field $f_\psi^{\boldsymbol{M}}(\mathcal{H})$ on a given map $\boldsymbol{M}$ (def. V) such that $\Psi[\mathtt{I}^*] = \Psi_\uparrow$, and $f_\mathtt{r}^{\boldsymbol{M}}(\mathcal{H}[\mathtt{I}^*]) = \mathtt{I}$. Then the top $k \ll |\mathcal{H}|$ ranked pose hypotheses $\mathcal{H}[\mathtt{I}^*]_{0:k-1}$ define set $\mathcal{V}$ such that $\psi_0 = \max f_\psi^{\boldsymbol{M}}(\mathcal{H}[\mathtt{I}^*]_{0:k-1})$, and for all $\hat{\boldsymbol{p}}_\mathcal{V} \in \mathcal{V}$ and any $\hat{\boldsymbol{p}}_\mathcal{X} \in \mathcal{X}$: $f_\mathtt{r}^{\boldsymbol{M}}(\hat{\boldsymbol{p}}_\mathcal{V}) < f_\mathtt{r}^{\boldsymbol{M}}(\hat{\boldsymbol{p}}_\mathcal{X}) \Leftrightarrow f_\psi^{\boldsymbol{M}}(\hat{\boldsymbol{p}}_\mathcal{V}) < f_\psi^{\boldsymbol{M}}(\hat{\boldsymbol{p}}_\mathcal{X}) \Leftrightarrow \|\boldsymbol{p} - \hat{\boldsymbol{p}}_\mathcal{V}\|_2 < \|\boldsymbol{p} - \hat{\boldsymbol{p}}_\mathcal{X}\|_2$. By identifying the pose estimates that correspond to the bottom k CAER values, this rationale attempts to recover the identity of the pose hypotheses with the bottom k pose errors across $\mathcal{H}$. It constitutes the core of the proposed passive global localisation method, termed CBGL, and is described in pseudocode in Algorithm II.

Assuming the satisfaction of Observation O, the challenge is choosing such k, $d_{\boldsymbol{l}}$, and d_α that, given pose estimate error requirements $\delta_{\boldsymbol{l}}$, δ_θ (def. VII; hyp. H), CBGL produces admissible pose estimates while being executed in timely manner. Given the rank field's Monte Carlo nature, optimistically, the only option for increasing the accuracy of the final pose estimate by a factor of two is doubling the densities of the $\mathtt{r}$-field; instead of doing that—and thereby doubling the method's execution time—subsequent to the estimation of the pose estimates with the k lowest CAER values, CBGL utilises scan–to–map-scan matching [19], [20], followed by the estimation of the one pose estimate with the lowest CAER value within the group of matched estimates.

Matching allows for (a) the correction of the pose of true positive estimates by scan-matching the map-scan captured within the map from the pose of a pose estimate against the range scan measured by the real sensor, (b) by the same token the potential divergence of spurious, false positive, pose estimates, and hence their elimination as pose estimate candidates, (c) the production of finer pose estimates without excessive increase in execution time, and (d) the decoupling of the final pose estimate's error from the field's density. Selecting among all matched estimates the one with the minimum (updated) CAER allows for the system's delivery of one pose estimate response. Algorithms I, II, and III present the proposed method of CBGL in block diagram and algorithmic forms respectively.

V. Experimental Evaluation

This section serves the testing of Hypothesis H under state of the global localisation art methods and CBGL, in varying environmental conditions and sensor configurations. With regard to CBGL its three required parameters are set to $(d_{\boldsymbol{l}}, d_\alpha, k) = (40, 2^5, 10)$ after initial tests with the dataset used in subsection V-A. The rationale of choosing appropriate $d_{\boldsymbol{l}}, d_\alpha$ is depicted in figure 4, and k is chosen as such in order to retain a high-enough true positive discovery rate without significant increase in execution time (due to the application of scan–to–map-scan matching on k pose estimates). Furthermore references to sets $\mathcal{H}_*$ are made to lines 6, 9, and 13 of Algorithm I. All tests were performed with a processor of 12 threads and a clock speed of 4.00 GHz.

Algorithm I: `CBGL`

Input: $\mathcal{S}_R$, $\boldsymbol{M}$, $(d_{\boldsymbol{l}}, d_\alpha)$, k
Output: Pose estimate of sensor measuring range scan $\mathcal{S}_R$

$A \leftarrow$ `calculate_area(free(`$\boldsymbol{M}$`))`
$\mathcal{H} \leftarrow \{\varnothing\}$
for $i \leftarrow 0, 1, \ldots, d_{\boldsymbol{l}} \cdot A - 1$ **do**
  $(\hat{x}, \hat{y}, \hat{\theta}) \leftarrow$ `rand()`$: (x, y) \in$ `free(`$\boldsymbol{M}$`)`, $\hat{\theta} \in [-\pi, +\pi)$
  for $j \leftarrow 0, 1, \ldots, d_\alpha - 1$ **do**
    $\mathcal{H} \leftarrow \{\mathcal{H}, (\hat{x}, \hat{y}, \hat{\theta} + j \cdot 2\pi/d_\alpha)\}$
  end for
end for
$\mathcal{H}_1 \leftarrow$ `bottom_`k`_poses`$(\mathcal{S}_R, \boldsymbol{M}, \mathcal{H}, k)$ (Alg. II)
$\mathcal{H}_2 \leftarrow \{\varnothing\}$
for $k \leftarrow 0, 1, \ldots, |\mathcal{H}_1| - 1$ **do**
  $\hat{\boldsymbol{h}}' \leftarrow$ `sm2`$(\mathcal{S}_R, \boldsymbol{M}, \mathcal{H}_1[k])$ (Alg. III or e.g. `x1` [20])
  $\mathcal{H}_2 \leftarrow \{\mathcal{H}_2, \hat{\boldsymbol{h}}'\}$
end for
return `bottom_`k`_poses`$(\mathcal{S}_R, \boldsymbol{M}, \mathcal{H}_2, 1)$

Algorithm II: `bottom_`k`_poses`

Input: $\mathcal{S}_R$, $\boldsymbol{M}$, $\mathcal{H}$, k
Output: $\mathcal{H}_\triangledown$

$\Psi \leftarrow \{\varnothing\}$
for $h \leftarrow 0, 1, \ldots, |\mathcal{H}| - 1$ **do**
  $\mathcal{S}_V^h \leftarrow$ `scan_map`$(\boldsymbol{M}, \mathcal{H}[h])$
  $\psi \leftarrow 0$
  for $n \leftarrow 0, 1, \ldots, |\mathcal{S}_R| - 1$ **do**
    $\psi \leftarrow \psi + \left|\mathcal{S}_R[n] - \mathcal{S}_V^h[n]\right|$ (Eq. (1))
  end for
  $\Psi \leftarrow \{\Psi, \psi\}$
end for
$[\Psi_\uparrow, \mathtt{I}^*] \leftarrow$ `sort(`Ψ`, asc)`
$\mathcal{H}_\triangledown \leftarrow \{\varnothing\}$
for $h \leftarrow 0, 1, \ldots, k - 1$ **do**
  $\mathcal{H}_\triangledown \leftarrow \{\mathcal{H}_\triangledown, \mathcal{H}[\mathtt{I}^*[h]]\}$
end for
return $\mathcal{H}_\triangledown$

Algorithm III: `sm2`

Input: $\mathcal{S}_R$, $\boldsymbol{M}$, $\hat{\boldsymbol{p}}$
Output: $\hat{\boldsymbol{p}}$ + correction that aligns $\mathcal{S}_V^{\boldsymbol{M}}(\hat{\boldsymbol{p}})$ to $\mathcal{S}_R$

$\mathcal{S}_V \leftarrow$ `scan_map`$(\boldsymbol{M}, \hat{\boldsymbol{p}})$
$\boldsymbol{\Delta p} \leftarrow$ `scan-match`$(\mathcal{S}_R, \mathcal{S}_V)$ (e.g. `ICP` [21], `FSM` [22])
return $\hat{\boldsymbol{p}} + \boldsymbol{\Delta p}$

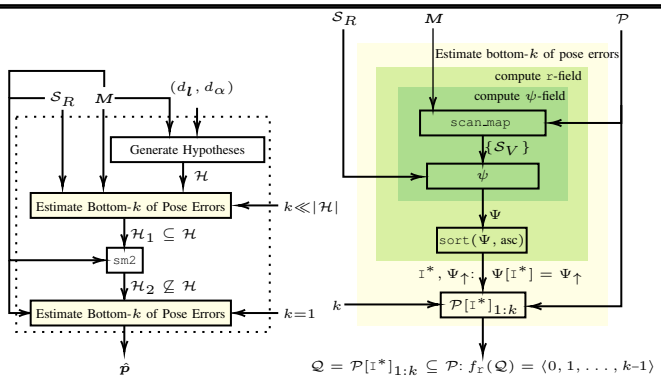

Fig. 3: CBGL in block diagram form. Left: Given a LIDAR's 2D measurement $\mathcal{S}_R$ and a map $\boldsymbol{M}$, CBGL generates a set of pose hypotheses $\mathcal{H}$ and estimates the k hypotheses with the least pose error (right; alg. II). Then it scan-to-map-scan matches those to $\mathcal{S}_R$ for finer estimation (`sm2`; alg. III). CBGL's output pose estimate is that with the least CAER among the k matched estimates. Right: CBGL's core method. Given $\mathcal{S}_R$, $\boldsymbol{M}$, and pose estimates $\mathcal{P}$, CBGL (a) computes and ranks the CAER values between $\mathcal{S}_R$ and map-scans captured from $\mathcal{P}$ within $\boldsymbol{M}$, and (b) outputs the hypotheses with the k lowest CAER values

A. Experiments in real conditions

The first type of test is conducted with the use of a Hokuyo UTM-30LX sensor, whose angular range is $\lambda = 3\pi/2$ rad and maximum range $r_{\max} = 30.0$ m, in the Electrical and Computer Engineering Department's Laboratory of Computer Systems Architecture (CSAL), Aristotle University of Thessaloniki, Greece, a map of which is depicted in figure 5. The sensor was mounted on a Robotnik RB1 robot, which was teleoperated to move within the environment while range scans were being captured. This resulted in $N_S = 6669$ range scans, whose number of rays are downsampled by a factor of four before being inputted to CBGL and ALS [23], an algorithm which implements Free-Space Features [24]. Other global localisation methods were not to tested for this type of experiment due to their infeasible execution time with respect to the range dataset's volume (see fig. 8). CBGL's internal scan–to–map-scan matching method is chosen to be PLICP [25] due to its low execution time and the sensor's non-panoramic field of view. The top of figure 6 depicts the proportion of output pose estimates from each method whose position and orientation error is lower than varying values of outlier thresholds $\delta_{\boldsymbol{l}}$, δ_θ; at the bottom they are depicted exclusively with regard to CBGL's output and its internal pose sets. The mean and standard deviation of the two methods' execution times are $(\mu_t^{\text{ALS}}, \sigma_t^{\text{ALS}}) = (6.15, 5.32)$ sec, and $(\mu_t^{\text{CBGL}}, \sigma_t^{\text{CBGL}}) = (1.61, 0.06)$ sec. From the experimental evidence it is clear that (a) hypothesis H is observed to be true 991 times out of a thousand for an outliers' locational threshold $\delta_{\boldsymbol{l}} = 0.5$ m when an angular threshold is δ_θ is not considered, and (b) CBGL outperforms ALS in terms of (i) number of pose estimates within all locational and angular thresholds and (ii) execution time.

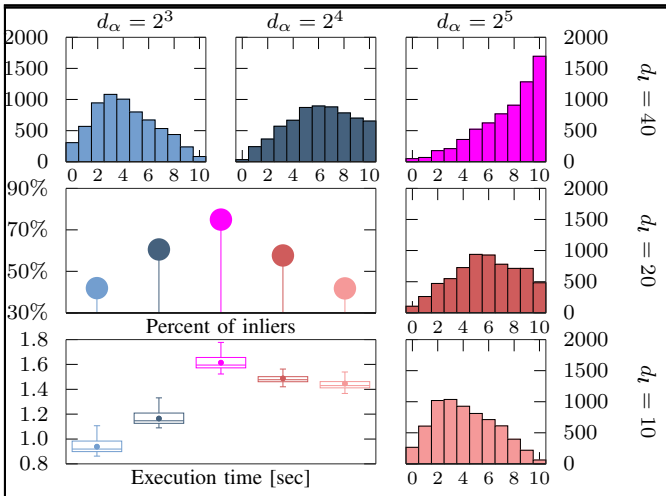

Fig. 4: Top row and right column: histograms of the number of times when exactly $n \in [0, k] = [0, 10]$ pose estimates belonging to set $\mathcal{H}_1$ exhibited pose errors lower than $\delta = (\delta_l^2 + \delta_\theta^2)^{1/2} = (0.3^2 + 0.4^2)^{1/2} = 0.5$ (m^2 + rad^2)$^{1/2}$. For densities $(d_l, d_\alpha) = (40, 2^5)$ this number is strictly increasing with n. Middle block: percent proportion of pose estimates whose pose error is lower than δ for varying field densities. Bottom block: the distribution of corresponding execution times

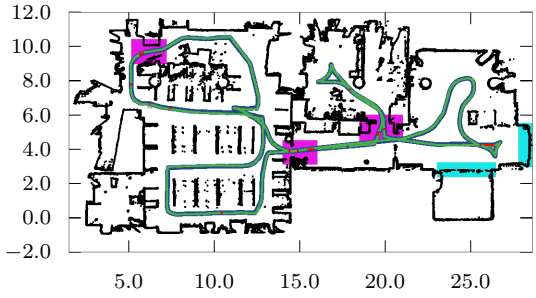

Fig. 5: The map of the CSAL environment (black), the trajectory of the sensor (blue), and CBGL's estimated positions of the sensor (green). Sensor poses for which CBGL's output exhibits position error larger than $\delta_l = 0.5$ m are marked with red, sources of great range noise with cyan, and regions around doors with purple. A total of $N_S = 6669$ pose estimations take place. Estimation is performed for each sensor pose independently of previous estimates and measurements

B. Simulations against sources of uncertainty

The second type of test concerns the main limiting factor of global localisation methods, i.e. uncertainty—:arising e.g. from spurious measurements, repeatability of surroundings, missing range information, or their combinations. For this reason the experimental procedure of [17] is extended here for the two methods tested therein, i.e. PGL-FMIC and PGL-PLICP, and then for CBGL, ALS, MCL [2], and GMCL [5]. Specifically these methods are tested against the two most challenging environments, i.e. WAREHOUSE and WILLOWGARAGE, in which a panoramic range sensor is placed at 16 different poses for $N = 100$ independent attempts at global localisation per tested method. The tests are conducted with the use of a sensor whose number of

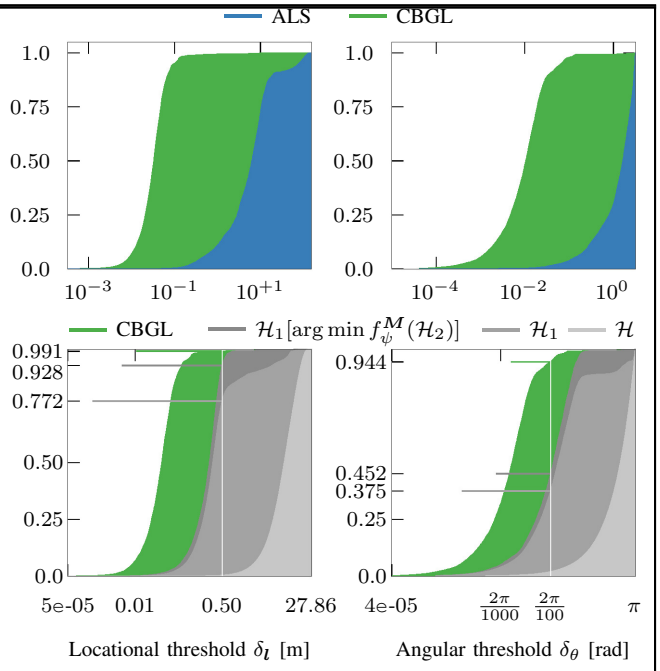

Fig. 6: Proportions of pose estimates whose position and orientation error is lower than corresponding thresholds δ_l and δ_θ. Top: ALS vs CBGL. Bottom: CBGL and internal pose estimate sets. Approximately 77% of all bottom-k pose estimates—the contents of $\mathcal{H}_1$ sets, populated via rank fields as described in sections II and IV—exhibit position errors lower than $\delta_l = 0.5$ m for $k = 10$, and so do over 99% of CBGL's final pose estimates. The improvement in position and orientation induced by scan–to–map-scan matching is captured by the difference between the output (i.e. $\mathcal{H}_2[\arg\min f_\psi^M(\mathcal{H}_2)]$) and $\mathcal{H}_1[\arg\min f_\psi^M(\mathcal{H}_2)]$

rays $N_s = 360$, maximum range $r_{\max} = 10.0$ m, and noise $\mathcal{N}(0, 0.05^2)$ [m,m^2]. CBGL's internal scan–to–map-scan matching method is chosen to be `x1` [20] due to the periodicity of the range signal, `x1`'s improved results over scan–to–map-scan matching state of the art methods, and its ability in matching scans captured from greater initial locational distances than ICP alternatives. The latter translates to the need for smaller initial hypothesis sets: for each environment the locational density is set to 3e+04 divided by the free space area of each environment. For Monte Carlo approaches MCL and GMCL the number of initial hypotheses is also set to 3e+04.

The maximum range of the sensor is such that the geometry of environment WAREHOUSE causes (disorderly) extended lack of sampling of the sensor's surrounding environment, which limits available information and may therefore produce spurious measurements and increase ambiguities between candidate estimates. In WILLOWGARAGE on the other hand, almost all sensor placements result in complete sampling of its surroundings, but the sensor is purposefully posed in such conditions as to challenge the localisation methods' ability to perform fine distinctions between similar surroundings. Figure 7 depicts the percentage of outputs whose position error is lower than $\delta_l = 0.5$ m per tested pose, and figure 8 depicts the overall distribution of execution

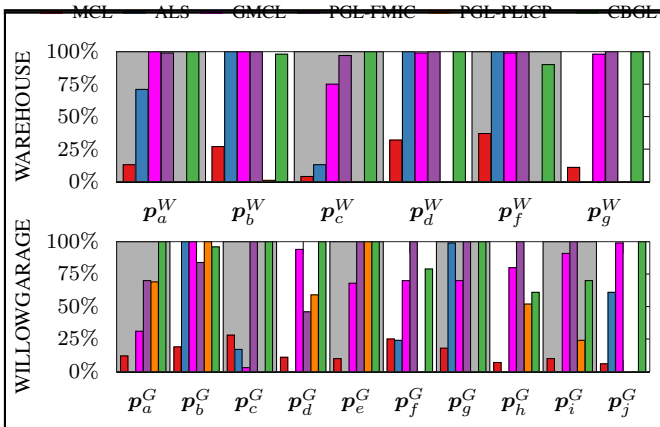

Fig. 7: Percent proportions of pose outputs whose position error is lower than $\delta_l = 0.5$ m per tested environment, pose, and method. Overall CBGL (green) features the highest number of inlier poses

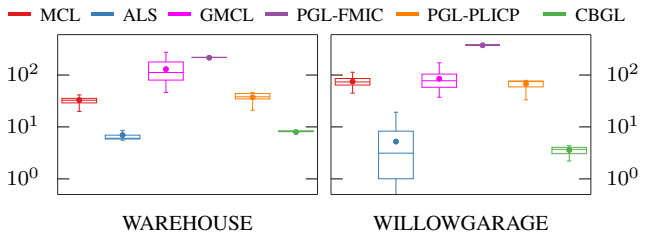

Fig. 8: Distribution of execution times per tested environment and algorithm in seconds for $N_s = 360$ rays. CBGL's execution time is at least eighteen times lower than other Monte Carlo approaches in WILLOWGARAGE and four times lower in WAREHOUSE

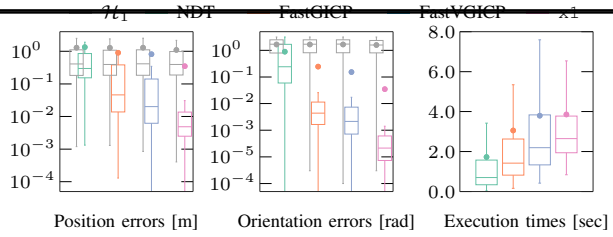

Fig. 9: Distributions of positional and orientational errors and of execution time of CBGL for varying choices of scan–to–map-scan matching methods. The errors of CBGL's internal $\mathcal{H}_1$ set are virtually unaffected by the decrease in angular range λ ($\lambda_{\text{NDT}} = \lambda_{\text{FastGICP}} = \lambda_{\text{FastVGICP}} = 3\pi/2 \neq \lambda_{\texttt{x1}} = 2\pi$)

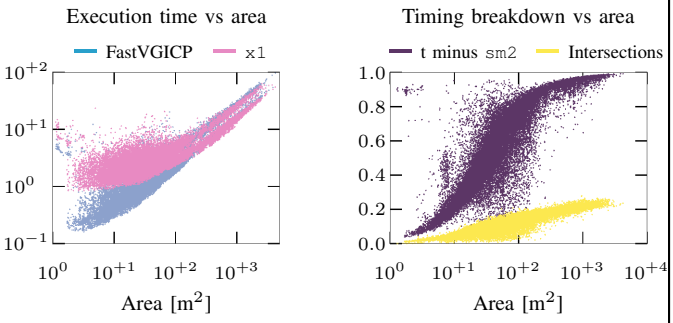

Fig. 10: Left: CBGL's execution time with respect to environment area for two choices of overlying scan–to–map-scan matching (sm2) methods. In rough terms $time_{CBGL}$ [sec] $= 17 \cdot 10^{-3} \cdot area$ [m^2]. Right: Proportion of CBGL $\circ$ x1's total execution time spent on (a) all operations up to and except for matching, and (b) computing map-scans, with respect to area

times per tested environment and algorithm. CBGL's mean execution time in environment WAREHOUSE is $\mu_t^W = 7.98$ sec and in WILLOWGARAGE $\mu_t^G = 3.59$ sec. Although the cardinality of set $\mathcal{H}$ is equal for both environments CBGL's execution times are uneven due to x1's increased execution time when dealing with scans with missing range information. Notwithstanding the aforementioned sources of uncertainty, CBGL manages to exhibit the highest number of inliers in each environment tested.

C. Simulations against environmental and algorithmic disparity

The third type of test aims to inquire how the performance of CBGL scales with respect to increasing environment area (and therefore to increased number of hypotheses), environment diversity, sensor angular range, and choice of overlying scan–to–map-scan matching method. CBGL is tested once in each of $N_E \simeq 4.5\text{e+}04$ environments, generated via the experimental procedure of [20], which utilises five established and publicly available benchmark datasets provided courtesy of the Department of Computer Science, University of Freiburg [26]. The coordinates of every map corresponding to each environment are corrupted by noise $\mathcal{N}(0, 0.05^2)$ [m, m^2]. The angular range of the range sensor varies according to the overlying scan–to–map-scan matching method used: for NDT [27], FastGICP [28], and FastVGICP [29]: $\lambda = 3\pi/2$ rad; for x1: $\lambda = 2\pi$ rad. Measurement noise is $\mathcal{N}(0, 0.03^2)$ [m,m^2]. As in subsection V-A the choice of field densities and k is $(d_l, d_\alpha, k) = (40, 2^5, 10)$.

Figure 9 illustrates that, with the exception of NDT, all versions of CBGL exhibit mean positional errors less than 1.0 m; its combination with x1 exhibits a mean error of approximately 0.5 m. The evidence support the claim that CBGL is robust to sensor angular range, as the distributions of errors are indistinguishable between bottom-k ($\mathcal{H}_1$) sets for $k = 10$.

Figure 10 shows the execution time of FastVGICP and x1 as a function of environmental area, and x1's timing breakdown with respect to (a) calculating up to line 9 of Algorithm I (that is CBGL's total time minus scan–to–map-scan matching time) and (b) computing map-scans, as proportions of total execution time. Given the evidence one may conclude that CBGL's execution time is linear with respect to environment area for areas larger than 200 m^2, with slope $l = 17\text{e-}03$.

VI. Characterisation & Limitations

Rank-fields produced by panoramic angular ranges induce fewer pose ambiguities than those produced by non-panoramic ones. In the latter case this means that (a) given the evidence of subsections V-A and V-C, where $\lambda = 3\pi/2$ rad, the choice of $k = 10$ largely inhibits the propagation of ambiguities to the output (fig. 9), and (b) increasing

values for k beyond that value may result in increased errors. However, non-panoramic angular ranges coupled with repeated environment structures may give rise to the conditions of figure 2 (bottom). Other sources of potential, large pose errors for CBGL are portrayed in figure 5: (a) regions encoded with cyan indicate closed glass doors, wherein great discrepancy with respect to map-derived virtual ranges may be observed, which is subsequently propagated to ψ-fields and hence $\mathtt{r}$-fields, and (b) regions encoded with purple indicate vicinities around doors, wherein the amount of environment and map information is restricted.

VII. Conclusion

REFERENCES

[1] M. Cooper, J. Raquet, and R. Patton, "Range Information Characterization of the Hokuyo UST-20LX LIDAR Sensor," *Photonics*, 2018.

[2] N. Akai, L. Y. Morales, and H. Murase, "Mobile Robot Localization Considering Class of Sensor Observations," in *2018 IEEE/RSJ International Conference on Intelligent Robots and Systems (IROS)*. IEEE, oct 2018, pp. 3159–3166.

[3] J. Wang, P. Wang, and Z. Chen, "A novel qualitative motion model based probabilistic indoor global localization method," *Information Sciences*, vol. 429, pp. 284–295, mar 2018. [Online]. Available: https://linkinghub.elsevier.com/retrieve/pii/S0020025517302347

[4] A. Yilmaz and H. Temeltas, "Self-adaptive Monte Carlo method for indoor localization of smart AGVs using LIDAR data," *Robotics and Autonomous Systems*, vol. 122, p. 103285, dec 2019. [Online]. Available: https://linkinghub.elsevier.com/retrieve/pii/S0921889019302106

[5] M. A. Alshikh Khalil and I. Hatem, "Development of a new technique in ros for mobile robots localization in known-based 2d environments," *Tishreen University Journal of Research and Scientific Studies - Engineering Sciences Series*, pp. 119–137, 2021.

[6] R. Chen, H. Yin, Y. Jiao, G. Dissanayake, Y. Wang, and R. Xiong, "Deep Samplable Observation Model for Global Localization and Kidnapping," *IEEE Robotics and Automation Letters*, vol. 6, no. 2, pp. 2296–2303, apr 2021. [Online]. Available: https://ieeexplore.ieee.org/document/9361285/

[7] F. Kallasi and D. L. Rizzini, "Efficient loop closure based on FALKO lidar features for online robot localization and mapping," in *2016 IEEE/RSJ International Conference on Intelligent Robots and Systems (IROS)*. IEEE, oct 2016, pp. 1206–1213. [Online]. Available: http://ieeexplore.ieee.org/document/7759202/

[8] M. Usman, A. M. Khan, A. Ali, S. Yaqub, K. M. Zuhaib, J. Y. Lee, and C.-S. Han, "An Extensive Approach to Features Detection and Description for 2-D Range Data Using Active B-splines," *IEEE Robotics and Automation Letters*, vol. 4, no. 3, pp. 2934–2941, jul 2019. [Online]. Available: https://ieeexplore.ieee.org/document/8716503/

[9] Z. Wang, L. Zhang, S. Zhao, and S. Zhang, "Global Localization With a Single-Line LiDAR by Dense 2D Signature and 1D Registration," *IEEE Sensors Journal*, vol. 21, no. 10, pp. 11 497–11 506, may 2021. [Online]. Available: https://ieeexplore.ieee.org/document/9184826/

[10] J. Meng, L. Wan, S. Wang, L. Jiang, G. Li, L. Wu, and Y. Xie, "Efficient and Reliable LiDAR-Based Global Localization of Mobile Robots Using Multiscale/Resolution Maps," *IEEE Transactions on Instrumentation and Measurement*, vol. 70, pp. 1–15, 2021. [Online]. Available: https://ieeexplore.ieee.org/document/9469927/

[11] R. W. M. Hendrikx, P. Pauwels, E. Torta, H. J. Bruyninckx, and M. J. G. van de Molengraft, "Connecting Semantic Building Information Models and Robotics: An application to 2D LiDAR-based localization," in *2021 IEEE International Conference on Robotics and Automation (ICRA)*. IEEE, may 2021, pp. 11 654–11 660. [Online]. Available: https://ieeexplore.ieee.org/document/9561129/

[12] S.-Y. An and J. Kim, "Extracting Statistical Signatures of Geometry and Structure in 2D Occupancy Grid Maps for Global Localization," *IEEE Robotics and Automation Letters*, vol. 7, no. 2, pp. 4291–4298, apr 2022. [Online]. Available: https://ieeexplore.ieee.org/document/9713689/

[13] K. Nielsen and G. Hendeby, "Survey on 2D Lidar Feature Extraction for Underground Mine Usage," *IEEE Transactions on Automation Science and Engineering*, vol. 20, no. 2, pp. 981–994, apr 2023. [Online]. Available: https://ieeexplore.ieee.org/document/9772692/

[14] T.-X. Xu, Y.-C. Guo, Z. Li, G. Yu, Y.-K. Lai, and S.-H. Zhang, "TransLoc3D : Point Cloud based Large-scale Place Recognition using Adaptive Receptive Fields," may 2021. [Online]. Available: http://arxiv.org/abs/2105.11605

[15] P. Yin, F. Wang, A. Egorov, J. Hou, Z. Jia, and J. Han, "Fast Sequence-Matching Enhanced Viewpoint-Invariant 3-D Place Recognition," *IEEE Transactions on Industrial Electronics*, vol. 69, no. 2, pp. 2127–2135, feb 2022. [Online]. Available: https://ieeexplore.ieee.org/document/9351776/

[16] J. Komorowski, "Improving Point Cloud Based Place Recognition with Ranking-based Loss and Large Batch Training," in *2022 26th International Conference on Pattern Recognition (ICPR)*. IEEE, aug 2022, pp. 3699–3705. [Online]. Available: https://ieeexplore.ieee.org/document/9956458/

[17] A. Filotheou, A. Tzitzis, E. Tsardoulias, A. Dimitriou, A. Symeonidis, G. Sergiadis, and L. Petrou, "Passive Global Localisation of Mobile Robot via 2D Fourier-Mellin Invariant Matching," *Journal of Intelligent & Robotic Systems*, p. 26, 2022.

[18] H. Yin, X. Xu, S. Lu, X. Chen, R. Xiong, S. Shen, C. Stachniss, and Y. Wang, "A survey on global lidar localization: Challenges, advances and open problems," *arXiv:2302.07433*, 2023.

[19] G. Vasiljević, D. Miklić, I. Draganjac, Z. Kovačić, and P. Lista, "High-accuracy vehicle localization for autonomous warehousing," *Robotics and Computer-Integrated Manufacturing*, 2016.

[20] A. Filotheou, A. L. Symeonidis, G. D. Sergiadis, and A. G. Dimitriou, "Correspondenceless scan-to-map-scan matching of 2D panoramic range scans," *Array*, 2023.

[21] I. Vizzo, T. Guadagnino, B. Mersch, L. Wiesmann, J. Behley, and C. Stachniss, "KISS-ICP: In Defense of Point-to-Point ICP Simple, Accurate, and Robust Registration If Done the Right Way," *IEEE Robotics and Automation Letters*, 2023.

[22] A. Filotheou, G. D. Sergiadis, and A. G. Dimitriou, "FSM: Correspondenceless scan-matching of panoramic 2D range scans," in *2022 IEEE/RSJ International Conference on Intelligent Robots and Systems (IROS)*. IEEE, 2022.

[23] N. Akai, "Reliable monte carlo localization for mobile robots," *arXiv:2205.04769*, 2022.

[24] A. Millane, H. Oleynikova, J. Nieto, R. Siegwart, and C. Cadena, "Free-Space Features: Global Localization in 2D Laser SLAM Using Distance Function Maps," in *2019 IEEE/RSJ International Conference on Intelligent Robots and Systems (IROS)*. IEEE, nov 2019, pp. 1271–1277.

[25] A. Censi, "An ICP variant using a point-to-line metric," in *2008 IEEE International Conference on Robotics and Automation*. IEEE, may 2008, pp. 19–25.

[26] "Datasets used in the experimental procedure." [Online]. Available: http://ais.informatik.uni-freiburg.de/slamevaluation/datasets.php

[27] P. Biber and W. Strasser, "The normal distributions transform: a new approach to laser scan matching," in *Proceedings 2003 IEEE/RSJ International Conference on Intelligent Robots and Systems (IROS 2003) (Cat. No.03CH37453)*, vol. 3. IEEE, 2003, pp. 2743–2748.

[28] A. Segal, D. Haehnel, and S. Thrun, "Generalized-ICP," in *Robotics: Science and Systems V*. Robotics: Science and Systems Foundation, jun 2009.

[29] K. Koide, M. Yokozuka, S. Oishi, and A. Banno, "Voxelized GICP for Fast and Accurate 3D Point Cloud Registration," in *2021 IEEE International Conference on Robotics and Automation (ICRA)*. IEEE, may 2021, pp. 11 054–11 059.